Instability in a cold atom interferometer

by

Daniel Pulido

A Thesis

Submitted to the Faculty

of the

WORCESTER POLYTECHNIC INSTITUTE

In partial fulfillment of the requirements for the

Degree of Master of Science

in

Applied Mathematics

by

May 2003

APPROVED:

Professor Mayer Humi, Major Thesis Advisor

Professor Alex A. Zozulya, Co-Advisor

Professor Bogdan Vernescu, Department Head

Abstract

In this thesis we present a theoretical anaylsis of the instability in a cold atom interferometer. Interferometers are often used to split a signal (e.g. optical beam, matter wave), where each part of the signal evolves separately, then the interferometer recombines the signal. Interference effects from the recombination can be used to extract information about the different environments that the split signal traversed. The interferometer considered here splits a matter wave, the wave function of a Bose-Einstein Condensate, by using a guiding potential and then recombines the matter wave. The recombination process is shown to be unstable and the nature of the instability is characterized.

Acknowledgements

It's been a pleasure working with my advisor Professor Zozulya. He has taught me, or more precisely, re-taught me quantum mechanics from scratch. Before meeting him, a "ket" or a "bra" seemed like an unholy and unnecessary abstraction. Now, I am loathe to write down an actual function, and am perfectly happy living in a abstract Hilbert space.

Coming from an engineering background, I should probably thank every professor in the math department, but especially Professors Humi, Larsen, and Martin whose classes helped to finally instill some mathematical rigor in me.

As for the non-PhD people, I should thank the entire chinese posse in the Math TA office. They have been at the bitter end of my wit for two years now, and they have kept me entertained. Also, I should give a shout out to Wilson and Dan for listening to my many theories about everything from God to why pop music is the end of us all.

I'd like to thank my friend and mentor Professor Emeritus Guido Sandri. Although not officially affiliated with this work, or any of my scholastic endeavors for that matter, our friendship, scientific collaborations, and our "almost" weekly meetings, which I have dubbed "Fridays with Guido", have been the proverbial shore in the tempest. Our fridays together have taught me about quaternions, physics, and life. They keep me alive.

I'd like to thank my parents Alfonso and Ines, and my sister Claudia, for letting

me not be a doctor and for letting me do things my own way, despite the fact that I'm sure that brings with it a maddening mixture of pain and joy.

Although I often choose solitude over mixed company, I am rarely alone in the company of my own thoughts, especially when I have people like this to think about. In other words, thanks folks.

Contents

List of Figures

Chapter 1

Introduction

1.1 Thesis Overview

In this thesis we present a theoretical anaylsis of the instability in a cold atom interferometer. Interferometers are often used to split a signal (e.g. optical beam, matter wave), where each part of the signal evolves separately, then the interferometer recombines the signal. Interference effects from the recombination can be used to extract information about the different environments that the split signal traversed. The interferometer considered here splits a matter wave, the wave function of a Bose-Einstein Condensate, by using a guiding potential and then recombines the matter wave. The condensate is initally trapped in a single well (parabola-like) potential and then split into two wells. The well separation allows the phase of the wave function to evolve independently in each well, which in turn causes interference upon recombination. The recombination process is shown to be unstable and the nature of the instability is characterized.

In Chapter 1 we give a brief history of Bose-Einstein Condensation (BEC). Chapter 2 presents the theoretical background of a BEC. Chapter 3 provides a description of the mathematical model used to study an atomic interferometer. Chapter 4 demonstrates the instability reported in this thesis and presents an analysis on

the nature of the instability. Chapter 5 summarizes the results and the Appendix describes the numerical methods used to solve the various computational problems encountered.

1.2 A Short History of Bose-Einstein Condensation

In the early 1920s Satyendra Nath Bose was studying the idea that the light came in discrete packets (photons). Bose gave a derivation of Planck's law, and to do so he postulated the rules for deciding when two photons should be counted as either identical or different. These rules have come to be known as "Bose-Einstein statistics" [1].

Einstein's name comes into the picture because Bose couldn't get his ideas published in the journals of the day, so he sent them to Einstein. Einstein liked the ideas, got them published, and extended on them. He postulated that the same rules might apply to atoms [2]. He found that a gas of bosons behaves rather different from a classical gas at very low temperatures. Below some critical temperature, a macroscopic fraction of the atoms occupy a single quantum state. Typical critical temperatures range from $20nK$ to $1\mu K$ [3]. This transition is known as a Bose-Einstein Condensation (BEC).

The BEC is unlike any other form of matter in the universe in that it behaves as a single quantum entity despite its size and density. A BEC's size can reach up to $1mm$ and typical experimental densities are as high as $10^{15} atoms/cm^3$. This is one reason why BEC's are being intensely studied because they might provide a useful means to test several fundamental issues of quantum mechanics. This thesis looks at one such experimental set up, a cold atom interferometer [17, 18].

After Einstein's treatment of an ideal gas of bosonic atoms, London (1938) considered the super-fluidity of helium as an example of BEC. The theory of BEC also led to the first successful analysis of super-conductivity [7]. Although BEC was predicted in 1924 [1, 2] it wasn't observed until 1995, in a series of experiments with clouds of magnetically trapped alkali atoms at JILA [4], MIT [5] and RICE [6]. BEC's are also being considered for use on cold atom guides and microchips [19, 20, 21, 22].

Chapter 2

BEC Theory

2.1 A Bose Gas

In this section we present an overview of a Bose gas and since this thesis examines the interference of matter waves, we will first give a brief qualitative explanation of what are matter waves.

In classical physics a particle has associated with it a position and momentum. However, this description is known to be incomplete. At the quantum mechanical level we associate wave-like properties to a particle. This comes by way of what is known as a wave function, which typically satisfies a Schrodinger type equation. The characteristic wavelength of the particle is given by the de Broglie wavelength,

$$\lambda = \frac{h}{mv}$$

where h is Planck's constant, m is the particle's mass, and v is the particle's velocity. However, these two seemingly paradoxical properties of classical particles and quantum mechanical waves are reconciled by the particle-wave duality. Namely, when a particle is detected, it is in fact a point-like particle that is detected, but the particle otherwise propagates like a wave. Consequently, all matter can be thought

of as a wave when we aren't looking, but as soon as you try and detect it, out comes a particle.

However, even though all matter has these wave-like properties, we don't experience them everyday because the typical de Broglie wavelength of matter is so small that it is beyond human perception. The table shows the typical wavelength of various physical processes that are described by waves.

Typical wavelengths (meters)	
AM Radio	100
Sound	1
Light	10^{-6}
Matter waves	10^{-10}

Therefore, the wave nature of matter waves only becomes evident when explaining microscopic physics. However, since BEC is concerned with matter at very cold temperatures (micro-Kelvins) it deals with matter waves with long wavelengths. This is seen from the de Broglie relation where the wavelength of a particle is inversely proportional to it's velocity; and, since there is a direct relationship between the temperature, T, and the kinetic energy of a particle, $mv^2 = kT$, where k is Boltzmann's constant, then clearly $\lambda \propto \frac{1}{\sqrt{T}}$. So as the temperature is lowered the de Broglie wavelength is increased.

Bose-Einstein condensation is a quantum statistics phenomenon that occurs in a collection of bosons (particles with integer spin) when the de Broglie wavelength of the particles is greater than the average distance, d, between particles. Since λ is inversely proportional to square root temperature then $\lambda \backsim d$ occurs at some critical temperature, T_c.

For a thorough derivation of T_c see [13]. The critical BEC phase transition temperature is defined as the highest temperature at which a macroscopic number

of atoms occupy the lowest energy state. Einstein considered N non-interacting bosonic atoms in a box of volume L^3 with periodic boundary conditions. He showed that in the thermodynamic limit, given by $N, L \to \infty$ with $\frac{N}{L^3} = \rho = const$, a phase transition occurs at T_c given by $T_c = \frac{2\pi\hbar^2}{mk}\left(\frac{\rho}{\zeta(3/2)}\right)$, where ρ is the mean density of particles in the box and ζ is the Riemann zeta function.

In the BEC regime the atoms in the gas behave coherently, as one collectively wave. Therefore, a BEC of atoms differs from a classical gas of atoms much like laser light differs from light bulb. A classical gas (light bulb) contains atoms (photons) each of which has a different momentum, while in a BEC (laser), all the atoms (photons) have the same momentum, within the uncertainty principle. It is this collective behaviour that is described by a wave function governed by the Gross-Pitaevskii equation, derived in the next section.

2.2 Gross Pitaevskii Equation

In this section we derive the governing equation for a Bose-Einstein condensate [12]. We begin with the N-body Hamiltonian for a system of N bosonic atoms. Then, we employ the "mean field approximation", where an exact description of the N-body system is replaced with a single classical field. We also assume that there are no thermal excitations, which implies all the atoms are in the condensate. The resulting expression yields the Gross-Pitaevskii equation, a nonlinear Schrodinger equation which governs the evolution for the wave function of the condensate.

The N-body Hamiltonian for a collection of interacting bosons trapped by an

external potential V_{ext} is

$$\widehat{H} = \int d\mathbf{r}\widehat{\Psi}^{\dagger}(\mathbf{r}) \left[-\frac{\hbar^2}{2m}\nabla^2 + V_{ext}(\mathbf{r}) \right] \widehat{\Psi}(\mathbf{r}) + \frac{1}{2}\int d\mathbf{r}d\mathbf{r}'\widehat{\Psi}^{\dagger}(\mathbf{r})\widehat{\Psi}^{\dagger}(\mathbf{r}')V(\mathbf{r}-\mathbf{r}')\widehat{\Psi}(\mathbf{r}')\widehat{\Psi}(\mathbf{r}) \tag{2.1}$$

where $V(\mathbf{r}-\mathbf{r}')$ is the two-body inter-atomic potential and $\widehat{\Psi}^{\dagger}(\mathbf{r})$ and $\widehat{\Psi}(\mathbf{r})$ are the bosonic field operators that create and destroy a particle located at $\mathbf{r}$. All the properties of the system (e.g. ground state, time evolution) can be extracted from Eq. (2.1). However, calculating them directly from Eq. (2.1) can be analytically and computational burdensome for a large number of particles. Therefore, an alternative mean-field approximation, developed by Bogoliubov [11], is used to circumvent this problem. This approach not only simplifies the computational burden but it also simplifies the understanding of the physics of the problem by reducing the problem to just a few system parameters that have a simple physical interpretation.

The basic idea behind the mean-field approach is to factor out the contribution due to the condensate from the bosonic field operator, which is defined as a linear superposition given by $\widehat{\Psi}(\mathbf{r}) = \sum_i \Psi_i(\mathbf{r})a_i$, where $\Psi_i(\mathbf{r})$ are a complete set of orthonormal single particle wave functions (e.g. plane waves) and a_i are the particle destruction operators which destroy particles with the wave functio Ψ_i. The creation and destruction operators are defined in a Fock space by

$$a_i^{\dagger}|n_0, ..., n_i, ...\rangle = \sqrt{n_i + 1}|n_0, ..., n_i + 1, ...\rangle, \tag{2.2}$$

$$a_i|n_0, ..., n_i, ...\rangle = \sqrt{n_i}|n_0, ..., n_i - 1, ...\rangle, \tag{2.3}$$

where n_i is the number of atoms in state i and is the eigenvalue of $\widehat{n}_i = a_i^{\dagger}a_i$. They

also satisfy the commutation relations

$$\begin{aligned}\left[a_i, a_j^\dagger\right] &= \delta_{i,j}, \\ [a_i, a_j] &= 0, \\ \left[a_i^\dagger, a_j^\dagger\right] &= 0.\end{aligned}$$

The mean-field approximation then decomposes the field operator, in the Heisenberg representation, as

$$\widehat{\Psi}(\mathbf{r}, t) = \Psi(\mathbf{r}, t) + \widehat{\Psi}'(\mathbf{r}, t), \tag{2.4}$$

where $\Psi(\mathbf{r}, t) = \langle\widehat{\Psi}(\mathbf{r}, t)\rangle$ is a complex function and corresponds to the condensate wave function and $\widehat{\Psi}'(\mathbf{r}, t)$ destroys a particle not in the condensate. $\widehat{\Psi}'(\mathbf{r}, t)$ is a small perturbation with $\langle\widehat{\Psi}'(\mathbf{r}, t)\rangle = 0$. The evolution of the condensate wave function, $\Psi(\mathbf{r}, t)$, is derived from the Heisenberg equation of motion for the field operator $\widehat{\Psi}(\mathbf{r}, t)$ using the N-body Hamiltonian Eq. (2.1),

$$\begin{aligned} i\hbar\frac{\partial}{\partial t}\widehat{\Psi}(\mathbf{r}, t) &= [\widehat{\Psi}, \widehat{H}] && (2.5) \\ &= \left[-\frac{\hbar^2}{2m}\nabla^2 + V_{ext}(\mathbf{r}) + \int d\mathbf{r}'\widehat{\Psi}^\dagger(\mathbf{r}', t)V(\mathbf{r}' - \mathbf{r})\widehat{\Psi}(\mathbf{r}', t)\right]\widehat{\Psi}(\mathbf{r}, t) && (2.6)\end{aligned}$$

The interatomic potential used, $V(\mathbf{r}' - \mathbf{r})$, assumes only low-energy two-body collisions are dominant and they are characterized by the s-wave scattering length, a, which for a repulsive BEC is given by $a > 0$. The s-wave scattering length is the characteristic size of a particle that other particles experience when colliding with the particle. Therefore, we set

$$V(\mathbf{r}' - \mathbf{r}) = g\delta(\mathbf{r}' - \mathbf{r}), \tag{2.7}$$

where g is the interatomic interaction strength, defined as $g = \frac{4\pi\hbar^2 a}{m}$, $\hbar$ is Planck's constant, a is the scattering lenth, and m is the atomic mass.

Finally, since we assume that there are no thermal excitations and all the atoms are in the condensate, then we ignore the second term in Eq. (2.4) and then simply replace the quantum field operator with the classical field,

$$\widehat{\Psi}(\mathbf{r}, t) \rightarrow \Psi(\mathbf{r}, t), \tag{2.8}$$

which yields the Gross-Pitaevskii Equation,

$$i\hbar\frac{\partial}{\partial t}\Psi(\mathbf{r}, t) = -\frac{\hbar^2}{2m}\nabla^2\Psi(\mathbf{r}, t) + V(\mathbf{r})\Psi(\mathbf{r}, t) + g|\Psi(\mathbf{r}, t)|^2\Psi(\mathbf{r}, t). \tag{2.9}$$

The GPE is accurate assuming that a much smaller than then average inter-particle distance. In other words, the effective scattering size of each atom, is much smaller than the distance between atoms, so the only interactions occuring are atom-atom collisions. Also, using Eq. (2.8) is valid only at zero temperature. In other words, there are no thermal excitations of the gas and all the atoms remain in the condensate. However, the GPE is approximately valid as long as the temperature is well below the critical temperature required for a BEC transition to occur.

The use of GPE may seem puzzling at first since a wave function that was a function of the N position vectors of the N atoms has been replaced by a wave function that is a function of only one set of spatial coordinates. However, an intuitive justification is that an analogous procedure occurs in classical electro-magnetic theory, where a description of the individuals photons is foregone and is instead replaced by a single electro-magnetic field [15].

Chapter 3

Interferometer Model

3.1 Model Description

In this section we describe the mathematical model of the condensate interferometer to be analyzed later on [16, 17, 18]. The interferometric process is depicted in Fig. (3.1). Splitting a condensate into two parts is achieved using a time dependent guiding potential, V. The potential begins with a single well (i.e. parabolic). As the system evolves in time the singe well is split into two symmetric wells. The process of splitting the well is adiabatic. In other words it is slow enough so that higher modes of the potential are not excited.

The condensate splitting occurs in one dimension while motion along the other two dimension is tightly confined. The condensate is assumed to be initially in the weakly nonlinear ($N < 1$) ground state of the single well, which is a solution of

$$\mu\psi_0 = -\frac{\hbar^2}{2m}\nabla^2\psi_0 + V\psi_0 + g|\psi_0|^2\psi_0, \tag{3.1}$$

where μ is the chemical potential, that is, the amount of energy required to add or remove one atom from the BEC.

The potential is then adiabatically split into a double well. During separation,

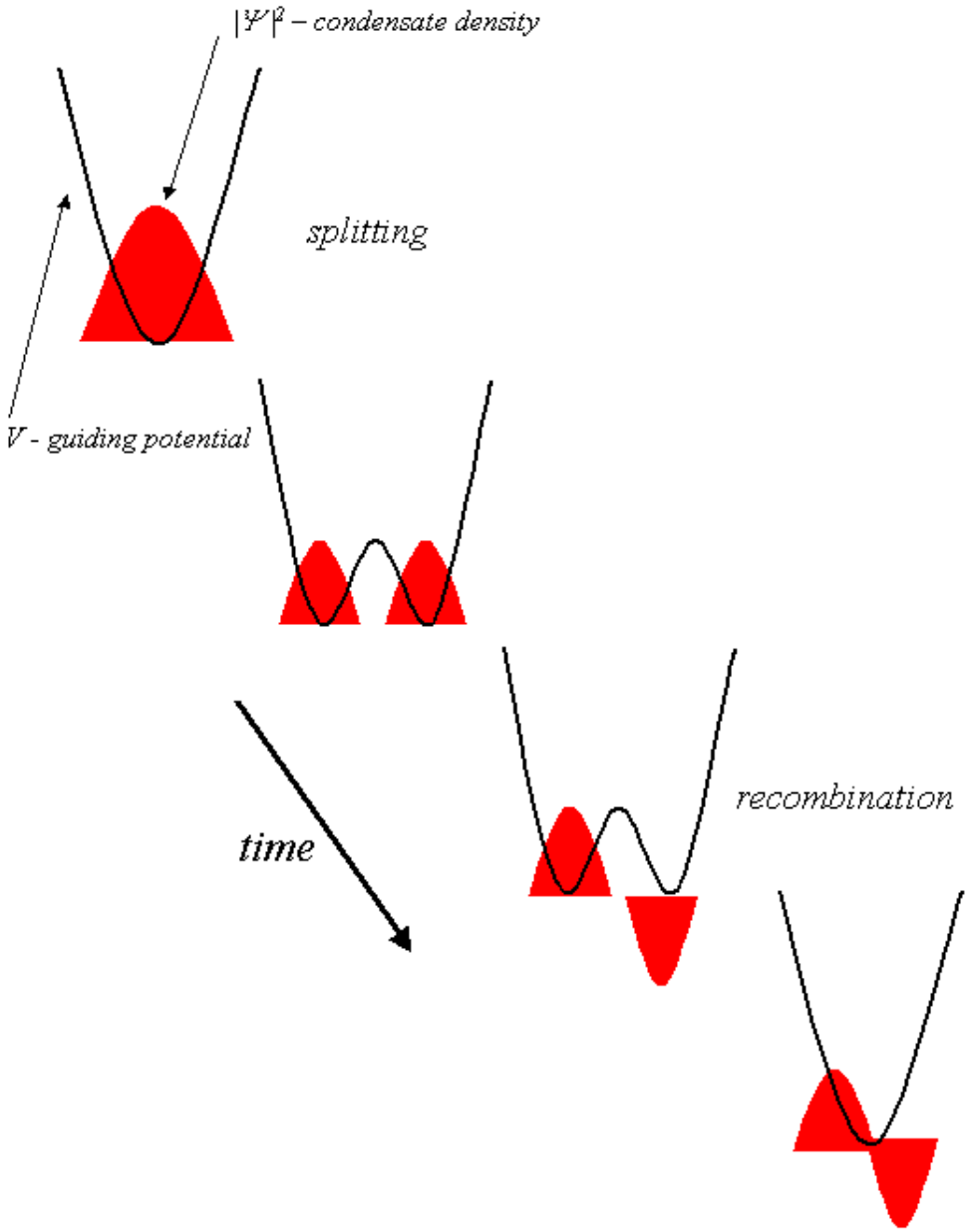

Figure 3.1: Schematic view of interferometer model.

the system evolves into a symmetric wave function that spreads over the two potential wells. Likewise, had the condensate been prepared in an anti-symmetric state, it would evolve into an anti-symmetric state that spreads out over the two wells. In other words, the separation process, as well as the recombination process, preserves the parity of the wave function, because the Hamiltonian is symmetric throughout the whole process. Therefore, it will not cause transitions between states of opposite symmetry.

The evolution of this one-dimensional BEC, in the mean-field approximation, is governed by a 1D GPE which is obtained by projecting the 3D GPE, Eq. (2.9), onto the lowest transverse mode of the linear guiding potential, $\phi_0(y,z)$, and which satisfies

$$\omega_0\phi_0 = -\frac{\hbar^2}{2m}\nabla_\perp^2\phi_0 + V_\perp(y,z)\phi_0,$$

where $\nabla_\perp^2$ is the two-dimensional Laplacian in the y and z directions and $V_\perp(y,z)$ is the potential used to trap the condensate in the transverse directions. To derive the governing 1D GPE, we begin by assuming the wave function is separable and of the form,

$$\psi_{3D}(x,y,z,t) = \phi_0(y,z)\psi_{1D}(x,t), \tag{3.2}$$

then substitute Eq. (3.2) into Eq. (2.9), multiply by $\phi_0^*(y,z)$ and integrate over the entire range of y and z. Now, using the orthonormality of the potential's eigenmodes,

$$\int_{-\infty}^{\infty} dy \int_{-\infty}^{\infty} dz |\phi_0|^2 = 1,$$

yields

$$i\hbar\frac{\partial}{\partial t}\psi(x,t) = -\frac{\hbar^2}{2m}\frac{\partial^2}{\partial x^2}\psi(x,t) + V(x,t)\psi(x,t) + gI|\psi(x,t)|^2\psi(x,t), \tag{3.3}$$

where

$$I = \int_{-\infty}^{\infty} dy \int_{-\infty}^{\infty} dz |\phi_0|^4,$$

and the $1D$ label has been dropped. The GPE considered in the analysis will actually be a non-dimensional form of Eq. (3.3),

$$i\hbar \frac{\partial}{\partial t'}\psi = -\frac{1}{2}\frac{\partial^2}{\partial x'^2}\psi + V'\psi + N|\psi|^2\psi \tag{3.4}$$

where the equation has been normalized by dividing through by $\hbar\omega_0$ and the new variables are given by,

$$\begin{aligned} x' &= \frac{x}{a_0}, \\ t' &= \omega_0 t, \\ V' &= \frac{V}{\hbar\omega_0}, \\ N &= \frac{g}{\hbar\omega_0}. \\ a_0 &= \left(\frac{\hbar}{m\omega_0}\right)^{\frac{1}{2}}. \end{aligned}$$

Also, from here on in the primes will be dropped.

The interferometer's splitting and recombination process is modeled in the guiding potential $V(x,t)$, Fig. (3.2). For our analysis we use a guiding potential of the form

$$V(x,t) = \left[1 + \left(\beta(t) - \frac{x^2}{2}\right)^2\right]^{\frac{1}{2}},$$

where $\beta(t)$ is a time dependent parameter that controls the separation of the two wells. Since the minima of $V(x,t)$ are at $x = \pm\sqrt{2\beta}$, then the separation distance of the two wells is given by $d = 2\sqrt{2\beta}$. This model was chosen because it easily

models the desired parabolic shape needed to split and recombine the condensate.

3.2 Adiabatic Recombination

The validity of the analysis that follows is based on the assumption that the interferometer model used is adiabatic. That is, the condensate is split and recombined slow enough so that modes not in the initial condensate are not excited. The parameters that characterize the guiding potential used were chosen to satisfy these requirements. The following is a brief explanation of the adiabatic theorem [14].

For a time dependent Hamiltonian, $H(t)$, which satisfies the Schrodinger equation

$$i\hbar\frac{\partial\psi}{\partial t} = H(t)\psi, \tag{3.5}$$

and has a given orthonormal, nondegenerate, discrete spectrum

$$H(t)\phi_n(t) = E_n\phi_n(t). \tag{3.6}$$

Given $\psi(t=0)$, then the solution of Eq. (3.5) can be written

$$\psi = \Sigma_n a_n(t)\phi_n(t) exp\left[-\frac{i}{\hbar}\int^t dt' E_n(t')\right]. \tag{3.7}$$

Substituting Eq. (3.7) into Eq. (3.5) and using the orthonormality of the eigenfunctions gives a system ODEs for the coefficients a_n,

$$\frac{\partial a_k}{\partial t} = \Sigma_{n\neq k} a_n\left[exp\left(\frac{i}{\hbar}\int^t dt'(E_k - E_n)(t')\right)\right]\frac{\int^t dt'\phi_k^*\left(\frac{\partial H}{\partial t}\right)\phi_n}{E_k - E_n}, \tag{3.8}$$

where $E_k = \hbar\omega_k$. This set of equation for all k's is equivalent to the Schrodinger equation, Eq. (3.5). Therefore, in order for additional modes to not be excited the

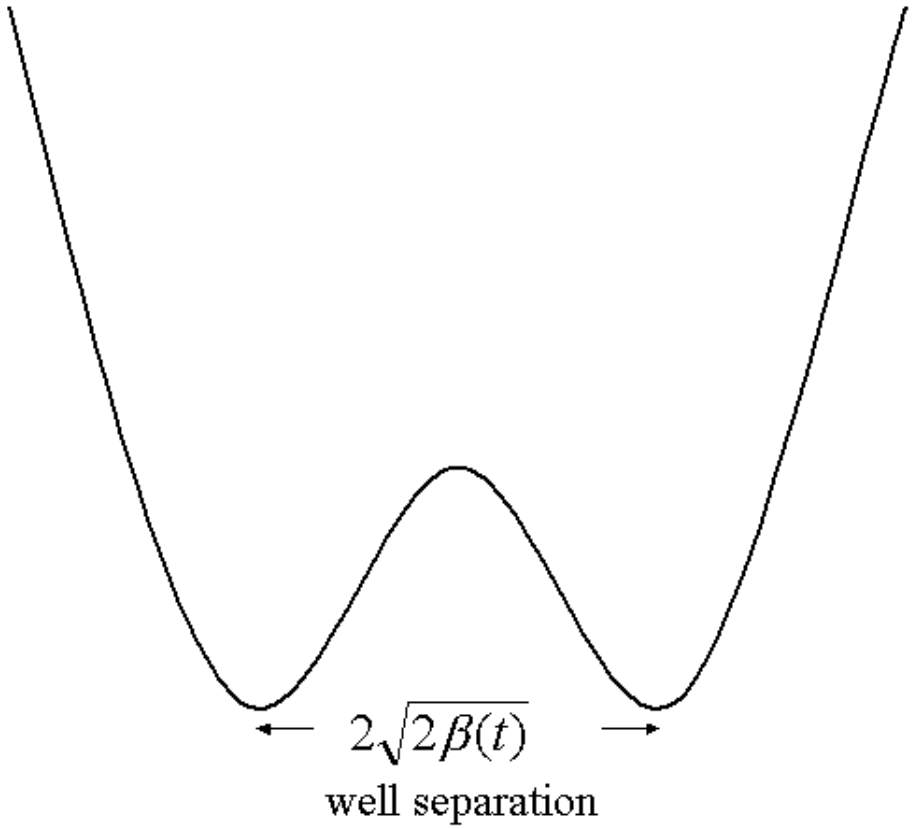

Figure 3.2: The potential well at time t.

adiabatic approximation requires all oscillating terms in Eq. (3.8) be negligible. In order to do so the last term in Eq. (3.8) must be much smaller than one. Consequently, the frequency differences $\omega_k - \omega_n$ must be larger than the inverse time associated with change in the system. So, if the wave function is placed in the k'th eigenstate of the initial Hamiltonian, then at time t it is in the k'th eigenstate of the Hamiltonian at time t. Therefore, th control parameter $\beta(t)$, must be chosen so that additional modes are not excited and the above criteria are met.

Chapter 4

Analysis

4.1 Interferometer Instability

In this section we demonstrate the instability that is present in the interferometer model. In order to do so we will simulate the recombination process and show the instability growth of one of the weak eigenmodes of the condensate. That is, when the condensate is split and recombined adiabatically, one expects that if the recombination is "slow" enough, then the condensate will map onto the appropriate eigenmode of the single well, where the "appropriate" eigenmode is defined later.

The condensate is initially taken to be in a singe well. That is, the condensate is taken to be initially in the lowest nonlinear mode of the potential

$$V(x,t) = \left[1 + \left(\beta(t) - \frac{x^2}{2}\right)^2\right]^{\frac{1}{2}},$$

with $\beta = 0$. Figure (4.1) shows this lowest eigenstate which satisfies,

$$\mu\psi_0 = -\frac{\hbar^2}{2m}\frac{\partial^2}{\partial x^2}\psi_0 + V\psi_0 + N|\psi_0|^2\psi_0, \tag{4.1}$$

and has an eigenvalue of $\mu = 1.4684$.

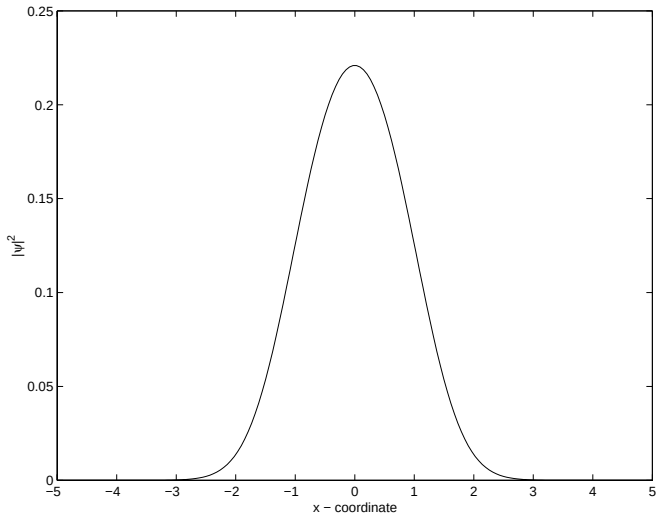

Figure 4.1: The lowest nonlinear single well mode.

Then β is increased and the condensate is spread out over the two wells. The separation is continued until there is a relative phase shift between the two wells close to π. Since β determines the separation between the two wells in the interferometer, the recombination process is modeled by using the following form for β,

$$\beta(t) = A \ln[\exp(-t/T) + 1], \tag{4.2}$$

where A and T are constants that determine the separation of the wells and the rate of recombination, respectively, and are chosen so as to ensure the process is adiabatic. The values $A = 3$ and $T = 90$ are used. Figure (4.2) shows that Eq. (4.2) allows both wells to merge linearly for $|t| \gg 0$.

Figure (4.3) shows the condensate density before and after the wells have recombined. However, due to the system's weak nonlinearity, prior to recombination this wave function is qualitatively similar to the first anti-symmetric linear mode of the

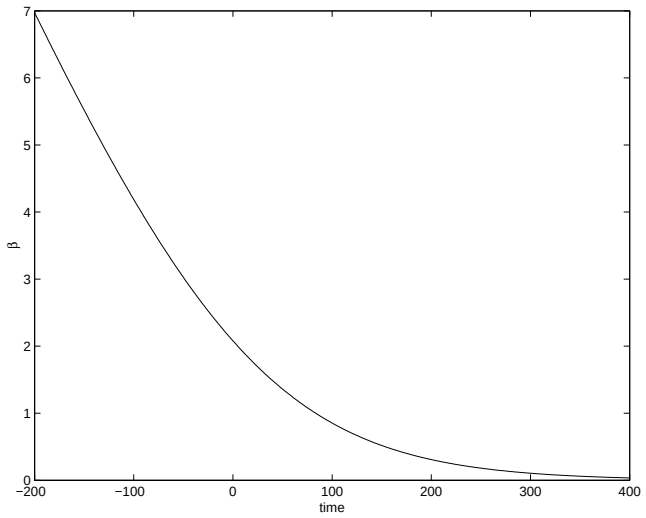

Figure 4.2: Recombination control parameter, β.

potential V, which satisfies

$$\lambda\phi_0 = -\frac{1}{2}\frac{\partial^2}{\partial x^2}\phi_0 + V\phi_0. \tag{4.3}$$

Since the recombination is adiabatic the wave function should map onto the lowest anti-symmetric mode of the single-well potential preserving its odd parity. However, Fig. (4.3) shows that this is not the case. Instead, the anti-symmetric parity is broken and the wave function is a combination of several modes. This break in symmetry is the instability observed and will be explained in the next section.

4.2 Modal Analysis

In this section we present an analysis of the instability of the interferometric recombination presented in the last section. The interferometer adiabatically splits the wave function into two wells with a guiding potential. The wave function then develops in each well independently. Consequently, the wave function in each well

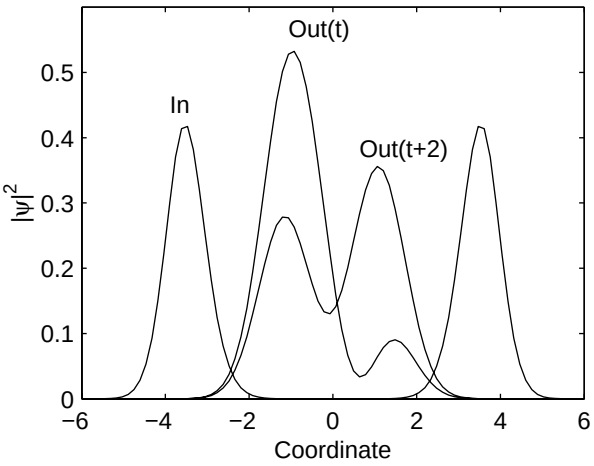

Figure 4.3: Condensate density before and after the recombination.

develops a different phase over time. This phase difference then produces interference upon recombination.

From the previous section, the condensate is loaded into the interferometer in the lowest (symmetric) nonlinear mode. The system then evolves and recombination is designed to occur when interference effects are at their greatest, namely when the phase difference is close to π. The condensate is then left predominantly in the first excited (anti-symmetric) state, but there's is still a small component due to the ground state. The instability will be shown to be caused by the weak nonlinear coupling of the strong first excited state to the weak ground state. The coupling causes the ground state to be amplified and depending upon it's initial strength it can potentially reach the same order of magnitude as the excited state. This instability is manifested in the anti-symmetry of the wave function being broken after recombination.

The evolution of the condensate is described by a 1D GPE.

$$i\frac{\partial}{\partial t}\psi(x,t) = \left[-\frac{1}{2}\frac{\partial^2}{\partial x^2} + V(x,t) + N|\Psi|^2\right]\psi(x,t). \tag{4.4}$$

where V is the guiding potential, time is normalized to the characteristic eigenfrequency ω_0 , x is normalized to the characteristic length $\left(\frac{\hbar}{\omega_0 m}\right)^{1/2}$, m is the atomic mass, and N is the normalized nonlinearity parameter.

In order to study the stability of the interferometer we perform a modal analysis on Eq. (4.4). First we decompose the wave function with a complete set of linear eigenmodes, $\phi_n(x,\beta)$, of the guiding potential which satisfy

$$\omega_n \phi_n(x,\beta) = -\frac{1}{2}\nabla^2 \phi_n(x,\beta) + V(x,t)\phi_n(x,\beta), \tag{4.5}$$

where ω_n are their associated eigenfrequencies and both $\phi_n(x,\beta)$ and ω_n parametrically depend on β . So, we set

$$\psi(x,t) = \sum_{n=0}^{\infty} A_n(t)\phi_n(x,\beta), \tag{4.6}$$

$$A_n(t) = \int dx \psi(x,t)\phi_n(x,\beta). \tag{4.7}$$

Substituting $\psi(x,t)$ into Eq. (4.4) gives a system of equations for the mode amplitudes

$$i\frac{d}{dt}A_n = \omega_n A_n + N\sum_{k,l,m} \kappa_{nklm} A_k A_l^* A_m, \tag{4.8}$$

where the overlap integrals are given by

$$\kappa_{nklm} = \int dx \phi_n \phi_k \phi_l \phi_m, \tag{4.9}$$

and they show the degree of overlap between different potential eigenmodes. Fig. (4.4) and (4.5) show the overlap integrals κ_{1111}, κ_{1122}, and κ_{2222}, and the difference in eigenfrequencies, $\omega_2 - \omega_1$, which will be the primary quantities of interest used in later sections. Both are easily computed from Eq. (4.5) with a second order

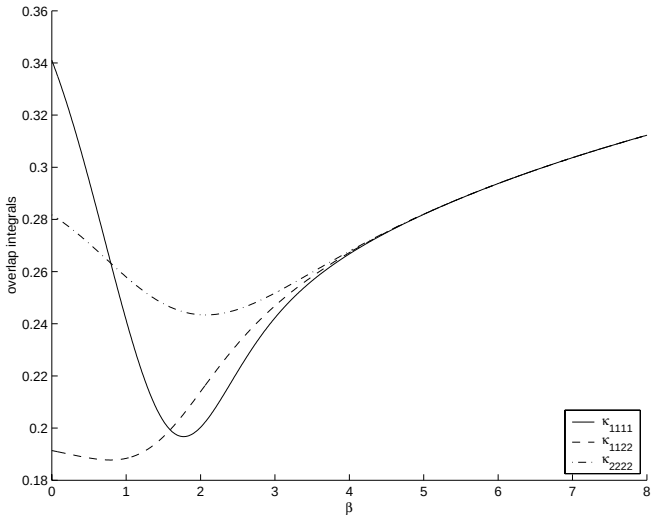

Figure 4.4: Overlap integrals.

discretization, where β is treated as a parameter.

Since upon recombination the condensate is predominantly in the lowest anti-symmetric nonlinear mode, then we expect that the primary contribution to the modal decomposition will be due to the lowest anti-symmetric linear mode, with a small perturbation being caused by the lowest symmetric mode. Therefore we assume that only two equations remain from Eq. (4.8)

$$i\frac{d}{dt}A_1 = \omega_1 A_1 + N\kappa_{1111}|A_1|^2 A_1 + 2N\kappa_{1122}|A_2|^2 A_1 + N\kappa_{1122}A_2^2 A_1^*, \quad (4.10)$$

$$i\frac{d}{dt}A_2 = \omega_2 A_2 + N\kappa_{2222}|A_2|^2 A_2 + 2N\kappa_{1122}|A_1|^2 A_2 + N\kappa_{1122}A_1^2 A_2^*. \quad (4.11)$$

In order to better demonstrate the instability presented in the last section, Eq. (4.10) and (4.11) were solved numerically for a number of cases. Figures (4.6) - (4.9) show the solutions of the modulus squared of the first two modal coefficients. A_1 is the coefficient for the first symmetric mode and A_2 is the coefficient for the first anti-symmetric mode. In order to model the case being considered we examine several

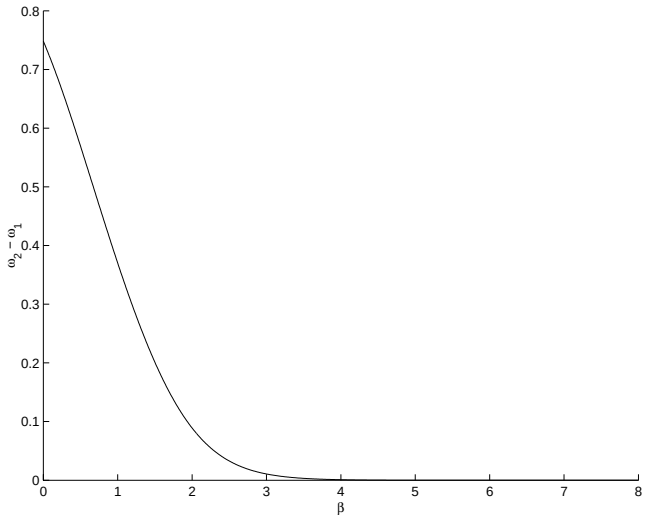

Figure 4.5: Difference of first two eigenfrequencies.

initial conditions $|A_1|^2(0) = 10^{-4}$, 10^{-5}, 10^{-7}, and 10^{-8}. $|A_2|^2(0)$ is determined from the normalization constraint $|A_1|^2 + |A_2|^2 = 1$.

All four figures show that $|A_1|^2$ grows exponentially during the initial recombination and then levels off as the condensate evolves in the single well, $t > 0$. However, Fig. (4.6) and (4.7) show that for sufficiently large initial values of $|A_1|^2$ the exponential growth of A_1 can cause it to grow to the same order of magnitude of the initially dominant mode, A_2. Also, Fig. (4.8) and (4.9) show that for sufficiently small initial values of $|A_1|^2$, even though A_1 grows exponentially, it levels off several orders of magnitude below A_2.

Whether or not the instability overwhelms the system clearly depends on the initialization of the condensate. In order to gain some insight on how to design an interferometer that avoids this instability we notice that the exponential growth seems to only occur during certain regions of the recombination; that is, the weak mode grows but then levels off. This indicates that the instability only occurs during certain values of the potential control parameter β. In order to verify this we

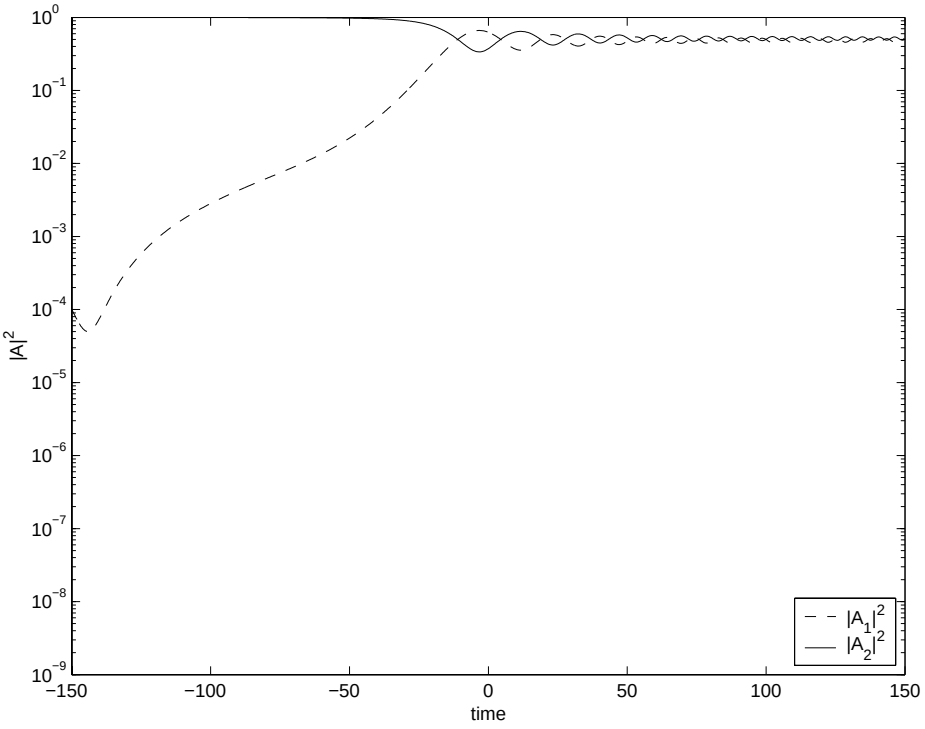

Figure 4.6: First two modal decomposition coefficients, $|A_1|^2(0) = 10^{-4}$.

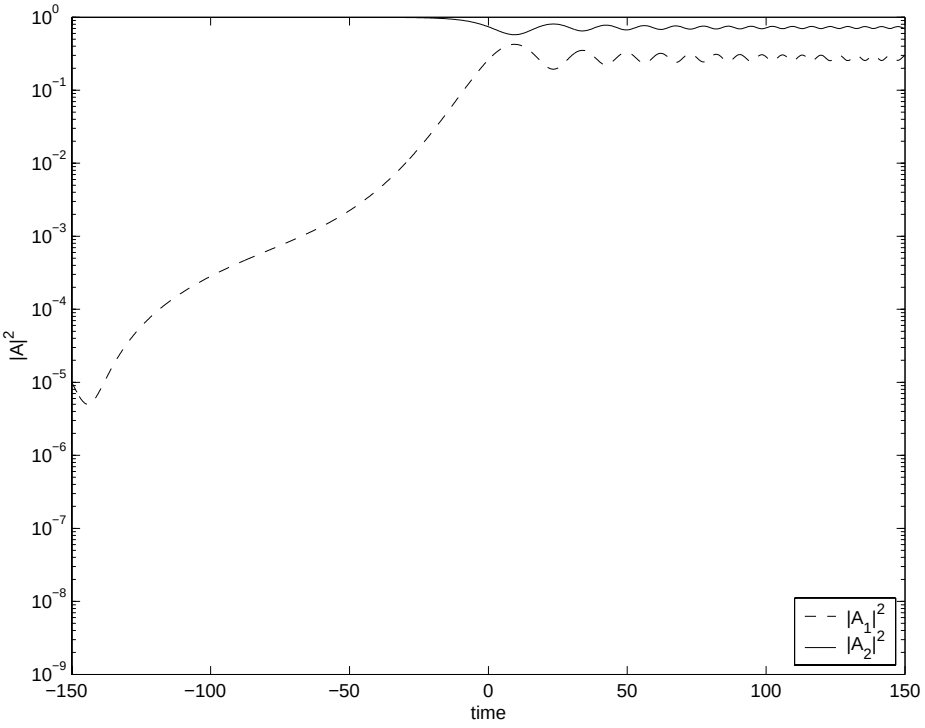

Figure 4.7: First two modal decomposition coefficients, $|A_1|^2(0) = 10^{-5}$.

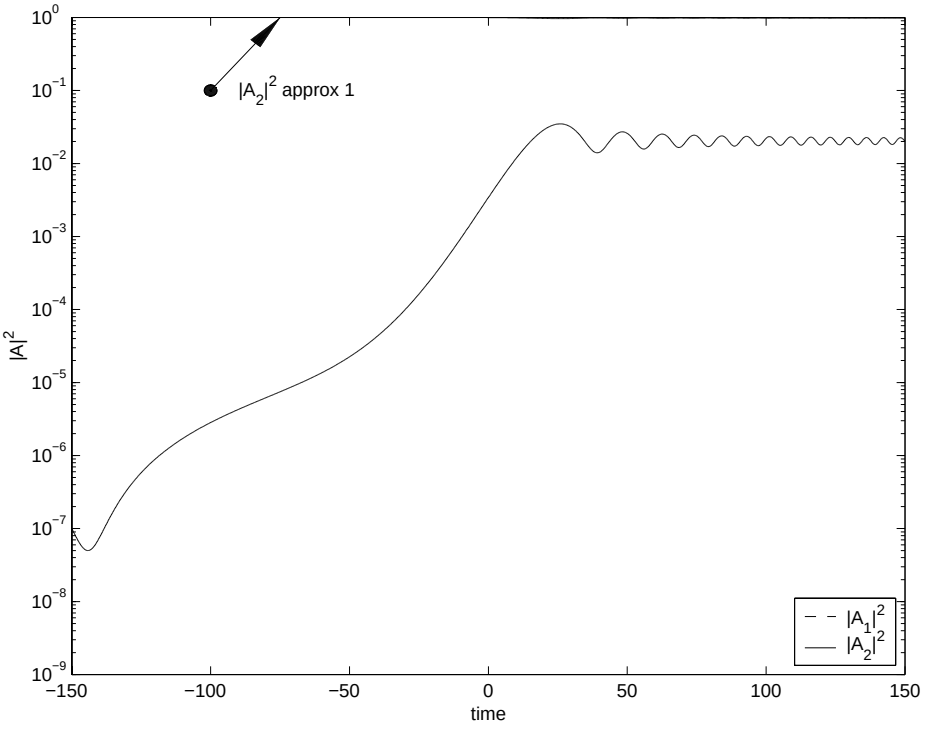

Figure 4.8: First two modal decomposition coefficients, $|A_1|^2(0) = 10^{-7}$.

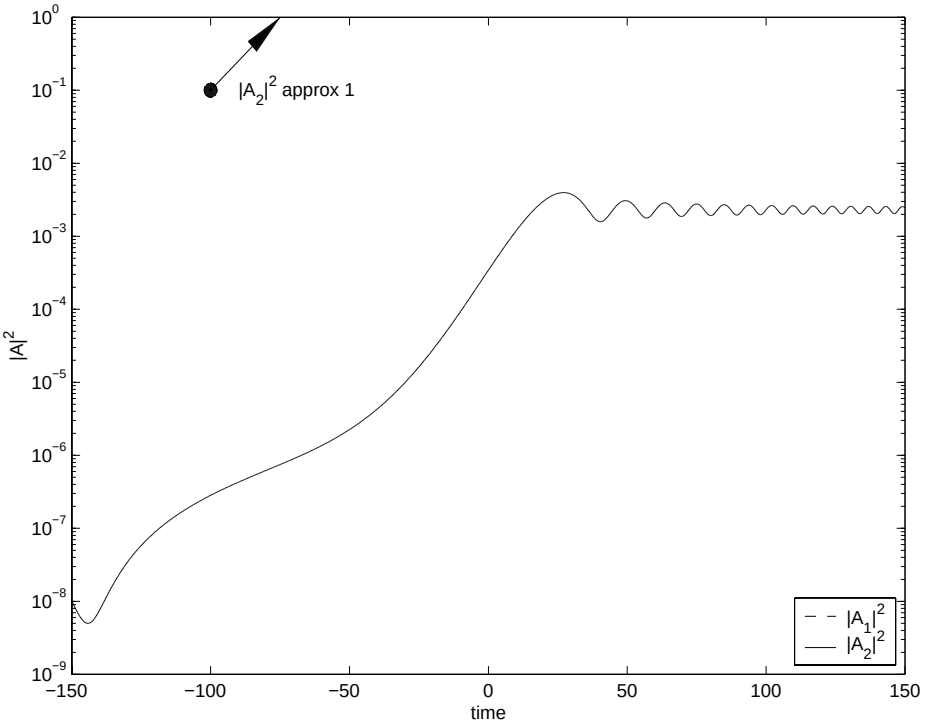

Figure 4.9: First two modal decomposition coefficients, $|A_1|^2(0) = 10^{-8}$.

compute the solutions of Eq. (4.10) and (4.11) for various fixed values of β. In other words, instead of modeling the recombination process dynamically, we will consider the static case where the two wells are running in parallel at a fixed distance, $2\sqrt{2\beta}$. Then the value of β is varied. Figures (4.10) - (4.17) show the solutions of $|A_1|^2$ and $|A_2|^2$ for $\beta = 0.5,\ 1.0,\ 1.5,\ 2.0,\ 2.5,\ 3.0,\ 3.5,$ and 4.0. The results show that for β values of about 2 to 3 $|A_1|^2$ has large oscillations, while below this region the solutions remain small and periodic. Above this region the solutions grow exponentially but the period of oscillation is large, thereby not giving the instability enough time to grow significantly. In order to precisely define this instability region the next section will solve for the growth rate of the weak mode as a function of β.

4.3 Stability Analysis

The growth rate of the instability is computed here by both a rigorous perturbation of Eq. (4.4) and a simpler approximation to the modal equations Eq. (4.10) and (4.11). However, both methods give qualitatively similar results, although the former has a wider range of applicability.

To compute the growth rate we assume that the instability is caused by a small perturbation $\delta(x,t)$, which perturbs the large first anti-symmetric eigenmode, $\phi(x)$. Therefore, let

$$\psi = (\phi(x) + \delta(x,t))\, e^{-i\mu t}, \tag{4.12}$$

and substitute into

$$i\frac{\partial}{\partial t}\psi(x,t) = \left[-\frac{1}{2}\frac{\partial^2}{\partial x^2} + V(x,t) + N|\Psi|^2\right]\psi(x,t). \tag{4.13}$$

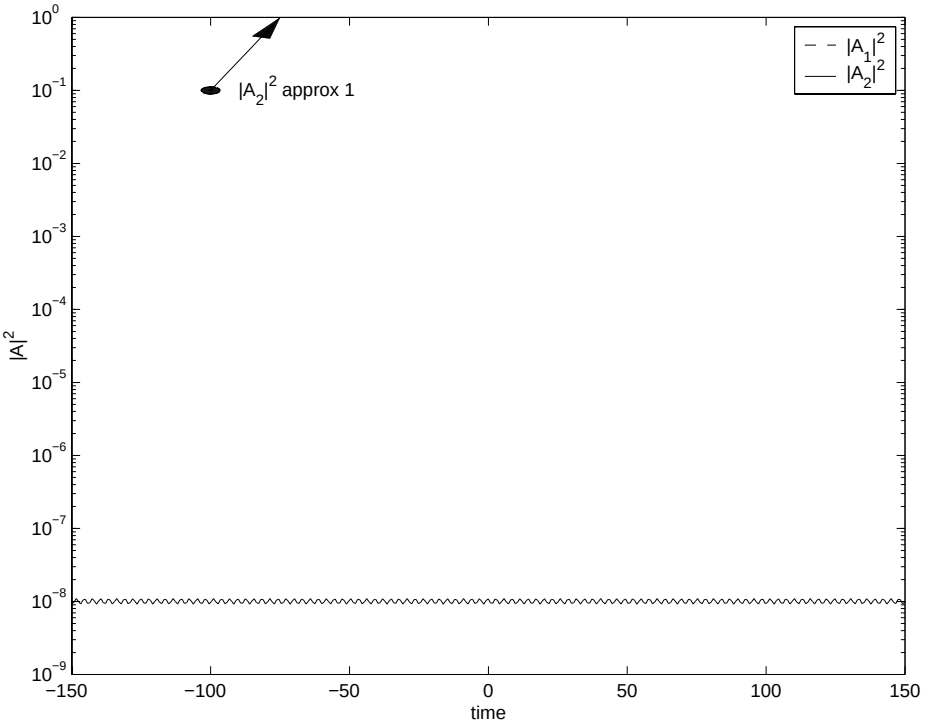

Figure 4.10: First two modal decomposition coefficients, $\beta = 0.5$.

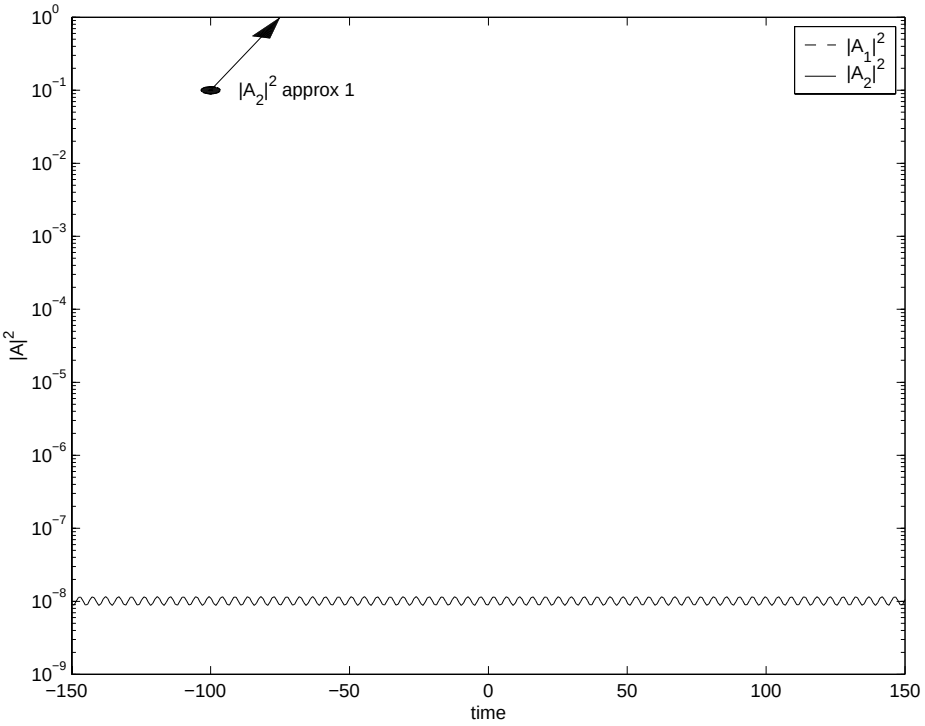

Figure 4.11: First two modal decomposition coefficients, $\beta = 1.0$.

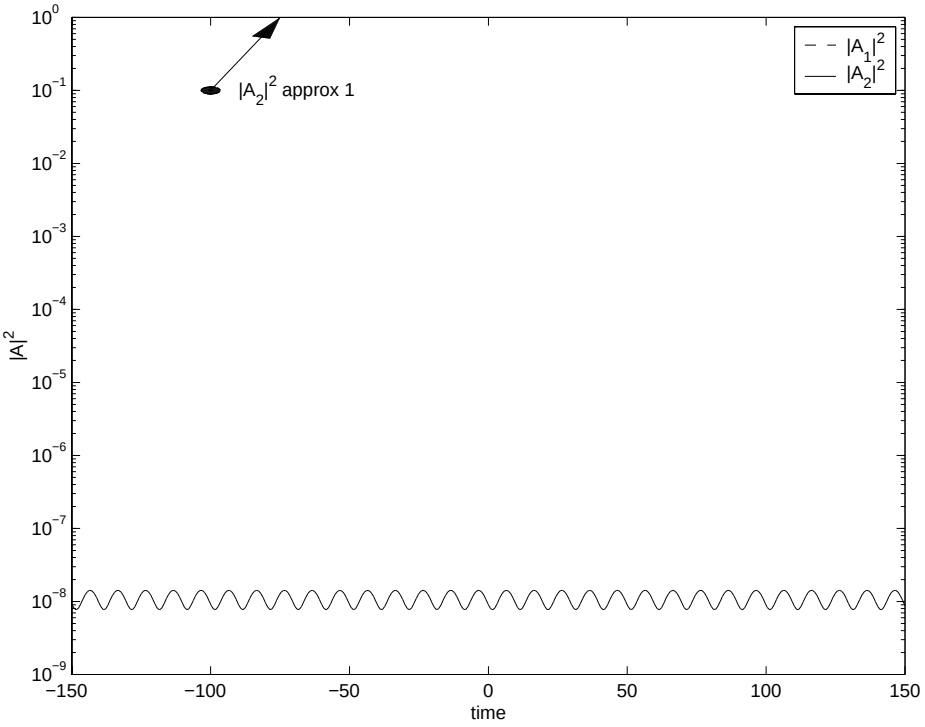

Figure 4.12: First two modal decomposition coefficients, $\beta = 1.5$.

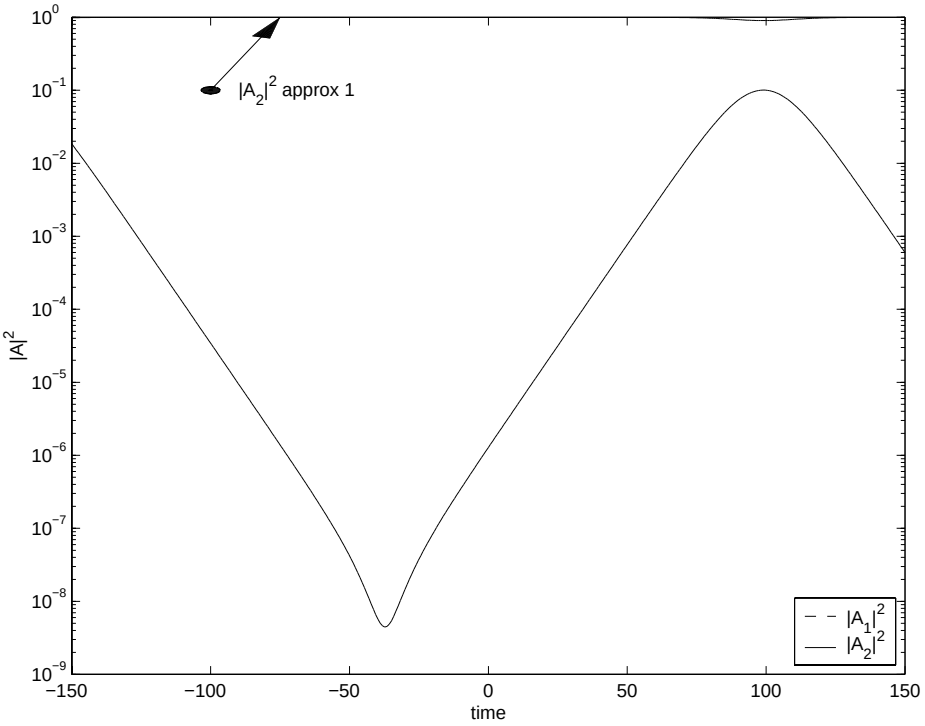

Figure 4.13: First two modal decomposition coefficients, $\beta = 2.0$.

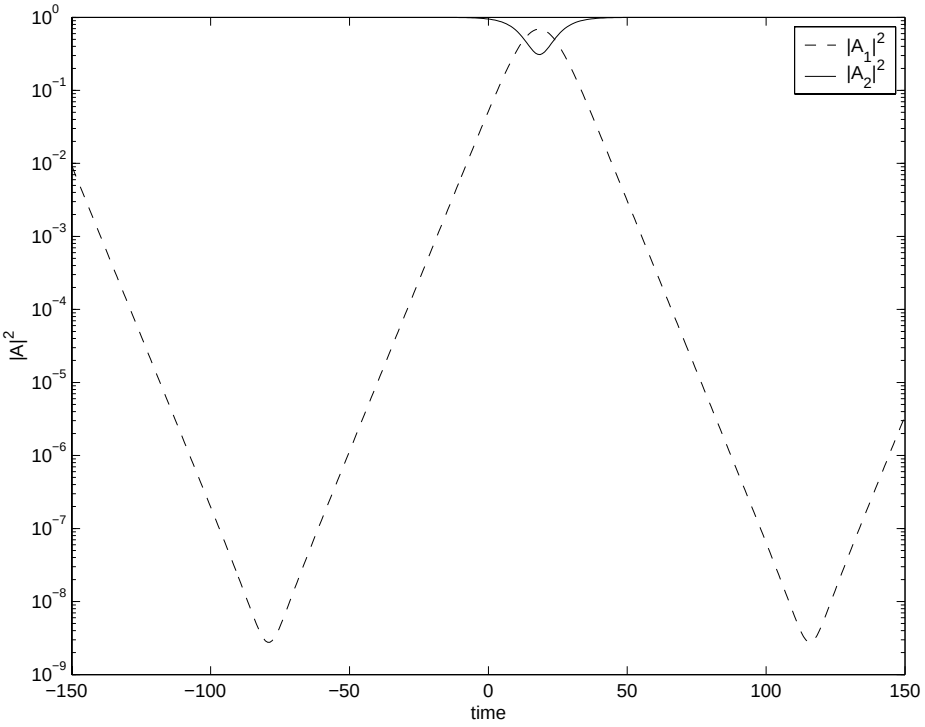

Figure 4.14: First two modal decomposition coefficients, $\beta = 2.5$.

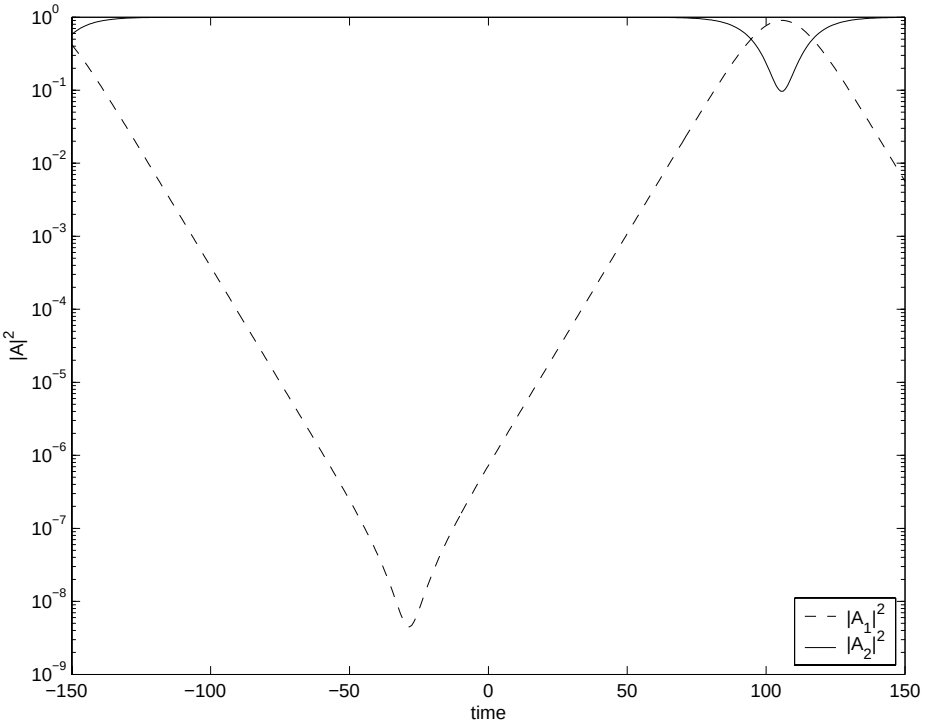

Figure 4.15: First two modal decomposition coefficients, $\beta = 3.0$.

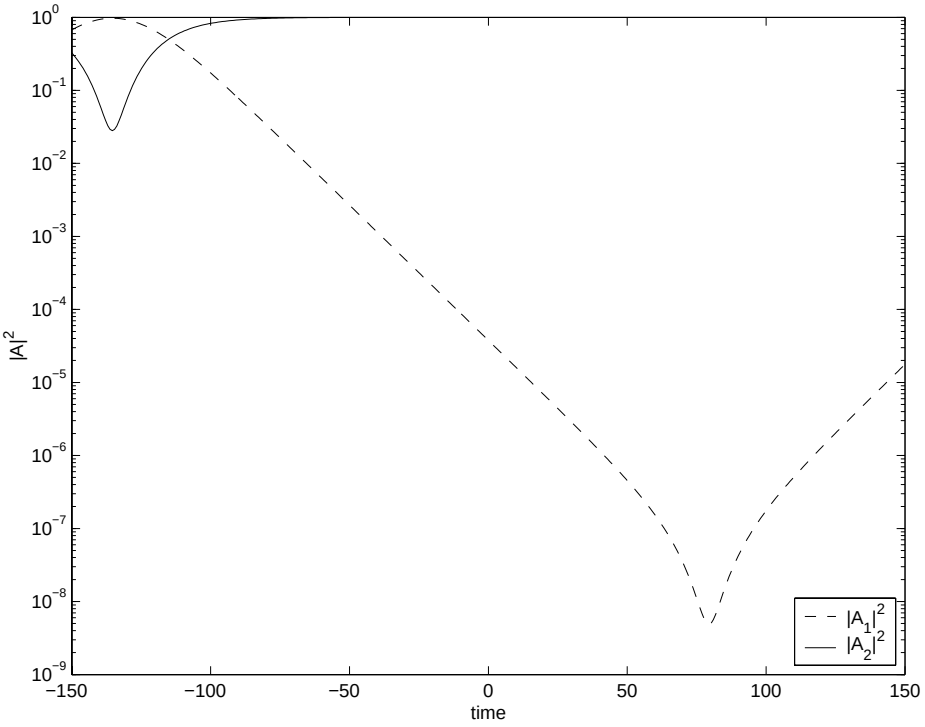

Figure 4.16: First two modal decomposition coefficients, $\beta = 3.5$.

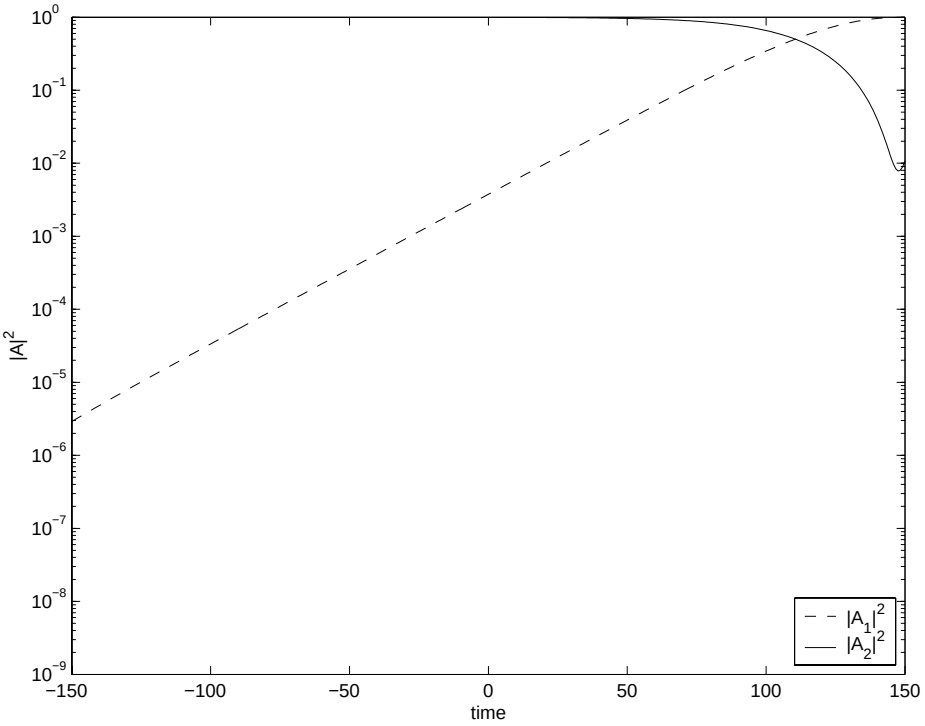

Figure 4.17: First two modal decomposition coefficients, $\beta = 4.0$.

Equating the zeroth order terms yields,

$$\mu\phi(x) = \left[-\frac{1}{2}\frac{\partial^2}{\partial x^2} + V(x,t) + N|\phi|^2\right]\phi(x), \tag{4.14}$$

and first order terms yield

$$i\frac{\partial}{\partial t}\delta(x,t) = -\frac{1}{2}\frac{\partial^2}{\partial x^2}\delta(x,t) + \left(V + 2N|\phi|^2 - \mu\right)\delta(x,t) + \left(N\phi^2\right)\delta^*(x,t). \tag{4.15}$$

We solve for δ by assuming a solution of the form

$$\delta = (u(x) + iv(x))\, e^{\gamma t}, \tag{4.16}$$

and substituting into Eq. (4.15) then separating the real and imaginary parts yields,

$$\gamma u = -\frac{1}{2}\frac{\partial^2}{\partial x^2}v + \left(V + 2|\phi|^2 - N\phi^2 - \mu\right)v, \tag{4.17}$$

$$-\gamma v = -\frac{1}{2}\frac{\partial^2}{\partial x^2}u + \left(V + 2N|\phi|^2 + N\phi^2 - \mu\right)u. \tag{4.18}$$

These equations can be decoupled to yield

$$\gamma^2 u = a_1\frac{\partial^4}{\partial x^4}u + b_1\frac{\partial^2}{\partial x^2}u + c_1\frac{\partial}{\partial x}u + d_1 u, \tag{4.19}$$

$$\gamma^2 v = a_2\frac{\partial^4}{\partial x^4}v + b_2\frac{\partial^2}{\partial x^2}v + c_2\frac{\partial}{\partial x}v + d_2 v, \tag{4.20}$$

where

$$
\begin{aligned}
a_{1,2} &= -\frac{1}{4}, && (4.21)\\
b_{1,2} &= \frac{1}{2}\left(A_1 + A_2\right), && (4.22)\\
c_{1,2} &= \frac{\partial}{\partial x} A_{1,2}, && (4.23)\\
d_{1,2} &= \frac{1}{2}\frac{\partial^2}{\partial x^2} A_{1,2} - A_1 A_2, && (4.24)
\end{aligned}
$$

and

$$
\begin{aligned}
A_1 &= \left(V + 2N|\phi|^2 + N\phi^2 - \mu\right), && (4.25)\\
A_2 &= \left(V + 2N|\phi|^2 - N\phi^2 - \mu\right). && (4.26)
\end{aligned}
$$

The growth rate of the perturbation that we seek is γ, which can be solved by discretizing and solving either eigenvalue problem Eq. (4.19) or Eq. (4.20). Figure (4.19) shows the results of computing the growth rate of the instability using a fourth order discretization. However, discussion of the results will be postponed until the end of this section in order to first introduce a more immediate and simpler approach to computing γ for weak nonlinearities. The approach comes from solving the modal equations derived previously, Eq. (4.10) and (4.11), in the limit of interest (i.e. a weak symmetric mode).

In order to solve these equation we introduce new variables $y_1 = 2Re(A_1 A_2^*)$, $y_2 = 2Im(A_1 A_2^*)$, and $y_3 = |A_1|^2 - |A_2|^2$ which with Eq. (4.10) and (4.11) yield

$$
\begin{aligned}
\dot{y_1} &= -\Delta(1 - 2N_2 y_3) y_2,\\
\dot{y_2} &= \Delta(1 - 2N_1 y_3) y_1, && (4.27)\\
\dot{y_3} &= -2\Delta(N_2 - N_1) y_1 y_2
\end{aligned}
$$

where $\Delta = \Delta\omega + \frac{IN}{2}\Delta\kappa$, $\Delta\omega = \omega_2 - \omega_1$, $\Delta\kappa = \kappa_{2222} - \kappa_{1111}$, and I is an integration constant defined below. Clearly, since we have gone from a system of two complex equations, Eq. (4.10) and (4.11), to a system three real equations, Eq. (4.27), we have abandoned some information. From the definition of the new variables we can see that y_3 has no phase information while y_1 and y_2 are functions of the product of A_1 and the conjugate of A_2 so only their relative phase can be determined. Therefore, the absolute phase of the system is being ignored. However, since an overall phase factor of the eigenmodes can be ignored this does not present a problem. Equation (4.27) contains two integral constants which can be exploited to solve the system. The integrals are obtained from algebraic combinations of Eq. (4.27) and are given by

$$y_1^2 + y_2^2 + y_3^2 = I, \tag{4.28}$$

$$y_3 + N_1 y_1^2 + N_2 y_2^2 = C, \tag{4.29}$$

where I and C are constants to be determined from initial conditions and

$$\begin{aligned} N_1 &= \frac{N}{2\Delta}\left(\frac{\kappa_{1111} + \kappa_{2222}}{2} - 3\kappa_{1122}\right), \\ N_2 &= \frac{N}{2\Delta}\left(\frac{\kappa_{1111} + \kappa_{2222}}{2} - \kappa_{1122}\right). \end{aligned}$$

Now, we give an approximate solution of Eq. (4.27) in the limit of interest, where the amplitude of the first anti-symmetric, A_2, is much larger than the first symmetric mode, A_1 (i.e. $y_3 \approx 1$, y_1, $y_2 \ll 1$). This yields approximate exponential

solutions for y_1 and y_2,

$$\begin{aligned} y_1(t) &= y_1(0)e^{\gamma t}, \\ y_2(t) &= y_2(0)e^{\gamma t}, \end{aligned}$$

where

$$\gamma = \sqrt{-\Delta^2(1+2N_1)(1+2N_2)} \tag{4.30}$$

and an instability region is where the solutions diverge, that is, where the real part of γ is greater than 0. Imaginary solutions correspond to oscillatory stable solutions. Equation (4.30) is the weak nonlinear approximation to the eigenvalues of Eq. (4.10) and (4.11) that we seek. A plot of γ is shown in Fig. (4.18). The plot shows that there is a critical minimum value, $\beta_{min}(N)$ above which the recombination is unstable and there exists no critical maximum value after which the system is again stable. However, as β is increased the instability reaches a maximum and then falls off rapidly. So even though the system is always unstable above β_{min}, the instability past the maximum quickly becomes small. Therefore, for a condensate to be separated and then recombined β would initially be at zero (single well) then increased until a maximum value is reached, corresponding to the point of greatest separation of the two wells, then β is decreased again until recombination ($\beta = 0$). Consequently, β has to pass through this instability region. A simple remedy is to design the interferometer, through the control parameter β, so as to spend a minimum amount of time in the instability region as possible. However, since the model for the interferometer used here required the splitting and recombination to be adiabatic, these are two competing goals. In other words, the interferometer needs to be adiabatic, but not too adiabatic, in order to avoid the instability region.

Also, the above conclusions were drawn using the growth rate as computed from Eq. (4.30). However, Eq. (4.30) is only valid for weak nonlinearities, since letting N become large would make γ greater than zero for all values of β, leading to the conclusion that the system is unstable everywhere, even for a single well. However, using the more rigorus method which consists of solving either eigenvalue problem Eq. (4.19) or Eq. (4.20) and which is applicable to strong nonlinearities yields results, shown in Figure (4.19), which show similar behaviour to Fig. (4.18). The results show that even for strong nonlinearities, the system has a stable region, and above a critical well separation, the system becomes unstable. Again, the instability grows to a maximum and then tapers off. However, the rate at which the γ tapers off lessens for higher nonlinearities. Finally, many of the properties seen thus far concerning the behaviour and the instability of the wave function of the condensate have been drawn from numerical solutions of the 1D GPE, Eq. (4.4), and it's weakly nonlinear modal equivalent, Eq. (4.10) and (4.11). However, the wave function's instability can also be understood from the analytical solutions of Eq. (4.10) and (4.11), which are computed in the next section.

4.4 Analytical Solutions

This section provides some clarification for some of the behaviour seen in the numerics computed so far by finding exact solutions to the set of rewritten modal equations Eq. (4.27). Since two integral constants have been computed, Eq. (4.28) and (4.28), we only need to solve one of the equations from Eq. (4.27) to obtain the complete solution. For simplicity, we choose the third equation. Squaring the equation gives $\dot{y_3}^2 = 4\kappa_{1122}^2 y_1^2 y_2^2$. We can solve Eq. (4.28) and Eq. (4.29) for y_1 and

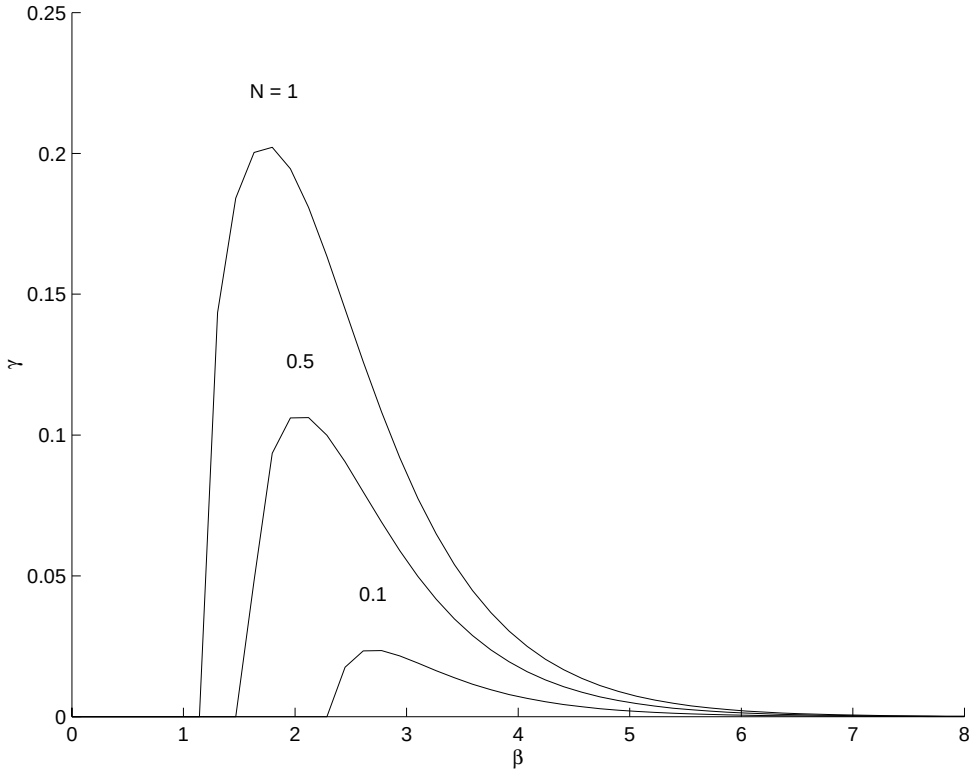

Figure 4.18: Growth rate, γ, modal decomposition.

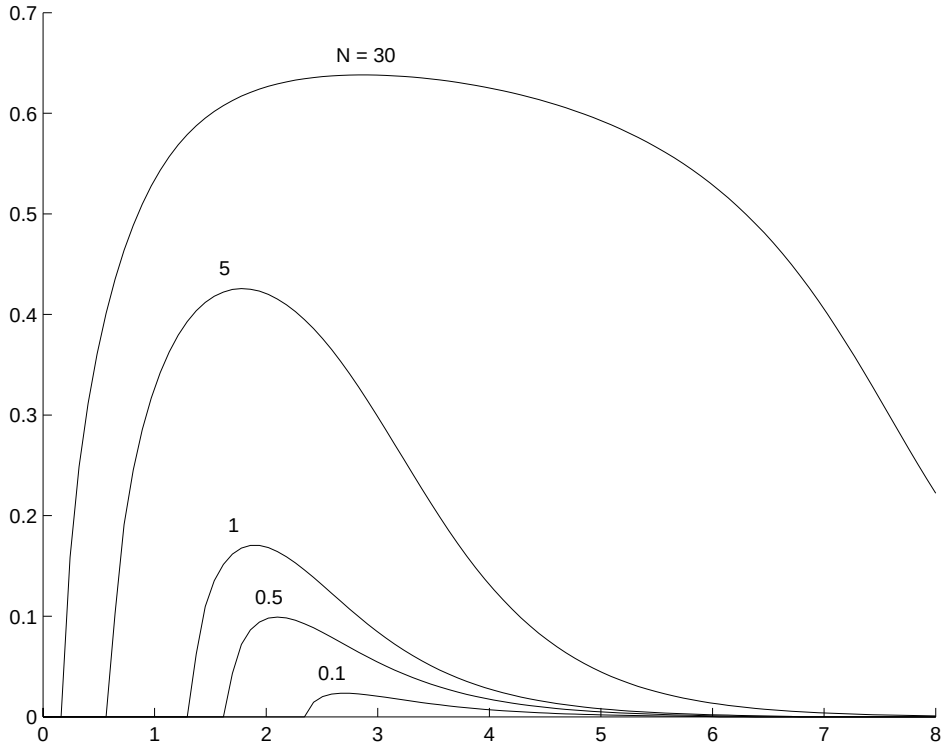

Figure 4.19: Growth rate, γ, rigorous perturbation.

y_2. These give

$$\begin{aligned}
\dot{y_1}^2 &= \frac{1}{(N_1-N_2)}[(N_1I^2-C)+y_3-N_1y_3^2], \\
\dot{y_2}^2 &= \frac{1}{(N_1-N_2)}[(C-N_2I^2)-y_3+N_2y_3^2], \\
\dot{y_3}^2 &= \frac{4\kappa_{1122}^2}{(N_1-N_2)^2}[(N_1I^2-C)+y_3-N_1y_3^2][(C-N_2I^2)-y_3+N_2y_3^2] \quad (4.31)
\end{aligned}$$

which for $\dot{y_3}$ gives a square root of a quartic polynomial in y_3. The solution of which in general is an elliptic function. The specific nature of the solution being given by the roots of the polynomial. Since y_3 determines the intensity of A_1 and A_2

$$|A_{1,2}|^2 = \frac{1}{2}(I \pm y_3) \quad (4.32)$$

where $I = |A_1|^2 + |A_2|^2 = const$, then the case being considered, where the condensate is initially in the lowest nonlinear mode of the single well potential, reduces to the initial conditions $y_3(0) \simeq \pm 1$ and $y_1(0), y_2(0) \simeq 0$, which imply $C = I$ and can be set to one. These reduce Eq. (4.31) to

$$\dot{y_3}^2 = \frac{4\kappa_{1122}^2}{(N_1-N_2)^2}N_1N_2[(y_3-a)(y_3-b)][(y_3-c)(y_3-d)] \quad (4.33)$$

where

$$\begin{aligned}
a, b &= \frac{1 \pm \sqrt{1+4N_1(N_1-1)}}{2N_1}, \\
c, d &= \frac{1 \pm \sqrt{1+4N_2(N_2-1)}}{2N_2}.
\end{aligned}$$

The type of elliptic function depends on the relation of $y_3(0)$ to the roots; a, b, c, and

d. There are clearly several solutions depending on the values of N_1 and N_2. For our present case, $y_3(0) \simeq \pm 1$, we have $N_1 < 0$ and $N_2 > 0$. This yields $a, c > 0 > b, d$; and even though there are four permutations of the possible positions of these roots the solution corresponding to each is of the same form. The general solution for any case $\alpha, \beta > y_3 > \gamma, \delta$ is given by

$$y_3 = \frac{\gamma - \delta C_1 sn^2(A_1 + B_1 t, k)}{1 - C_1 sn^2(A_1 + B_1 t, k)}, \tag{4.34}$$

where

$$\begin{aligned} A_1 &= sn^{-1}(\sqrt{\frac{(\beta-\delta)(y_3(0)-\gamma)}{(\beta-\gamma)(y_3(0)-\delta)}}, k), \\ B_1 &= \frac{\kappa_{1122}}{N_2 - N_1}\sqrt{-N_1 N_2}\sqrt{(\alpha-\gamma)(\beta-\delta)}, \\ C_1 &= \frac{\beta-\gamma}{\beta-\delta}, \\ k &= \sqrt{\frac{(\beta-\gamma)(\alpha-\delta)}{(\alpha-\gamma)(\beta-\delta)}}. \end{aligned}$$

The modulus, k, is a key parameter for elliptic functions as it determines it's generic behaviour. As $k \to 0$ an elliptic function behaves like a trigonometric function (e.g. $sn(x, 0) = sin(x)$) and as $k \to 1$ it behaves like a hyper-trigonometric function (e.g. $sn(x, 1) = sinh(x)$). Consequently, the instability region can also be understood from the general solutions of Eq. (4.27). For the same initial conditions as before (i.e. weak symmetric mode) the general solution for y_3, Eq. (4.34), is a ratio of elliptic $sn(t, k)$ functions. In Fig (4.20) the modulus of these functions is plotted as a function of the control parameter, β, for various nonlinearities. On comparing these results with Fig. (4.18), clearly, the regions of instability correspond to a drastic change in the modulus of the solutions. The modulus shifts from being very close to zero (trigonometric-like) to very close to one (hyper-trigonometric like)

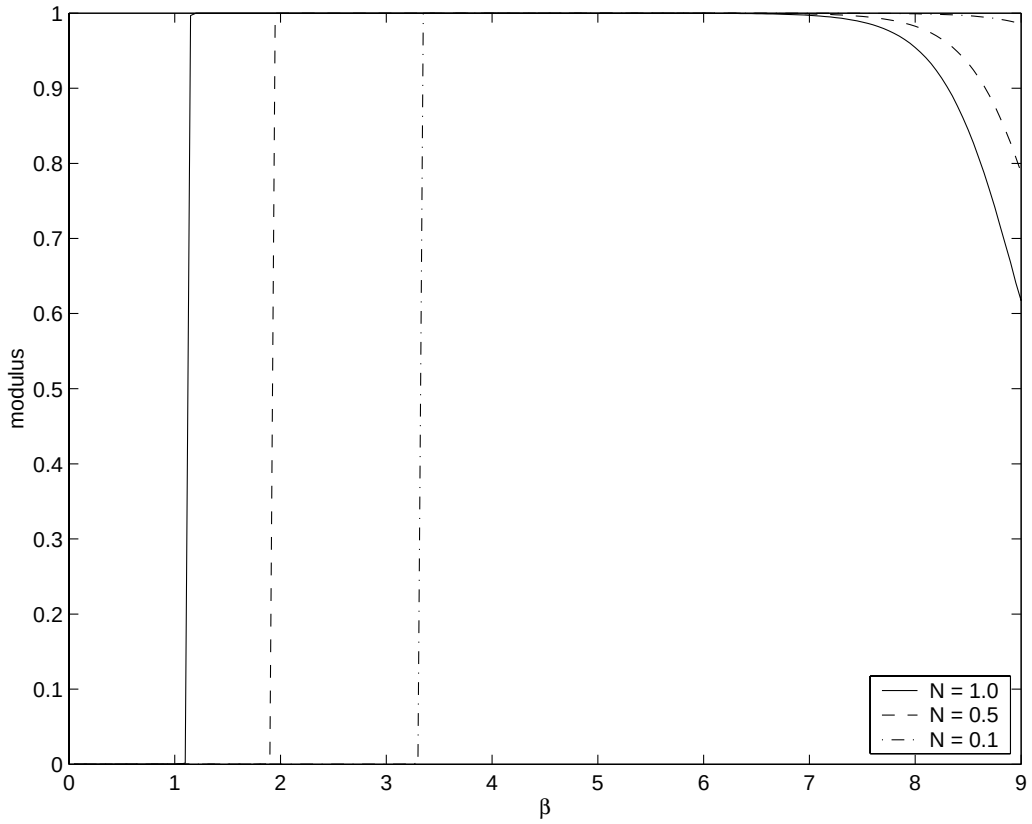

Figure 4.20: Modulus of elliptic function solutions.

and then back to zero. The instability region corresponds to the solutions behaving like hyper-trigonometric functions, which is evident in Fig. (4.13) through (4.17), where for $\beta \geq 2$ the solutions show exponential like growth. Also, as discussed previously, the exponential growth continues for larger β, but the effect on the instability is minimized because of the frequency and amplitude of the solutions. The frequency and amplitude are shown in Fig. (4.21) and (4.22). These clarify the trends shown previously in Figs. (4.10) through (4.17) where solutions for small values of β showed high frequency and small amplitudes, while as β was increased the frequency decreased and the amplitude increased.

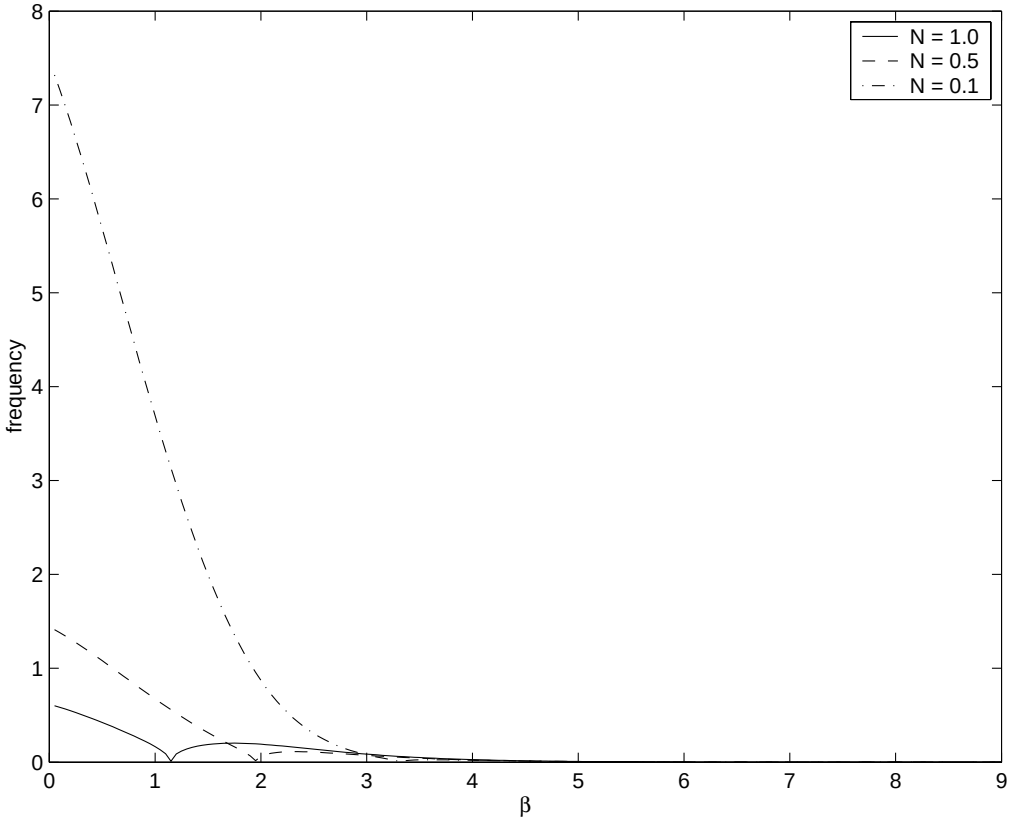

Figure 4.21: Frequency of elliptic function solutions.

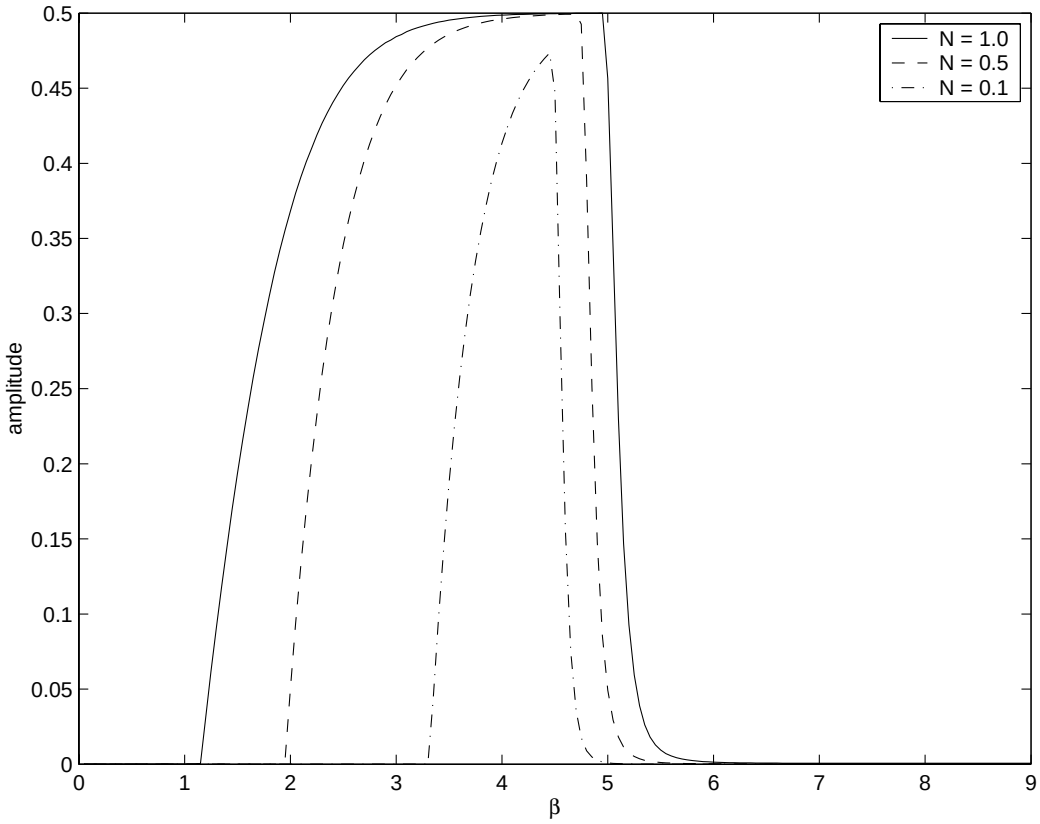

Figure 4.22: amplitude of elliptic function solutions.

Chapter 5

Conclusions

We have analyzed the performance of a cold atom interferometer. The analysis presented in Chpt. 4 shows that the interferometry of a Bose-Einstein Condensate can be potentially unstable. As the BEC matter wave is split and recombined by a guiding potential, there are unstable regions in the interferometer characterized by the distance between the split condensate. Below a critical separation the interferometer is stable, while above a certain separation it is unstable. The instability is caused by the exponential amplification of the initially weak ground state of the guiding potential. The amplification is caused by the nonlinear coupling of the initially strong first excited state to the ground state. The interferometry is done adiabatically (i.e. slow enough) so that the splitting and recombination process itself is not the cause of exciting unwanted modes. However, allowing the recombination to be done to slowly causes the condensate to spend too much time in the unstable region. Therefore, the remedy to eliminating this potential instability is to not make the interferometer too adiabatic, so as to spend the least amount of time possible in this unstable region.

Appendix A

Appendix: Numerical Methods

In this section we give a brief description of the numerical methods used to solve the various computational problems encountered in the subsequent analysis. The split-step Fourier method is discussed in regards to solving the 1D time-dependent GPE. Then the shooting method is briefly presented in relation to solving an eigenvalue problem of the time-independent 1D GPE.

A.1 Split-Step Fourier Method

Solving the one-dimensional version of Eq. (2.9) is made difficult because of the $|\psi|^2$ nonlinearity. As a result, in general the GPE has no analytical answer and must be solved numerically. One method is known as the Split-Step Fourier (SSF) Method. Eventhough the Hamiltonian in Eq. (2.9) is time dependent due to either V or $|\psi|^2$ being potentially time dependent, the SSF method assumes that those time variations are small enough, given a sufficiently small time interval, that we can treat H as constant over the time interval and directly integrate Eq. (2.9) to yield,

$$\psi_{n+1}(x, t + \Delta t) = exp(-i\Delta t H)\psi_n(x, t), \tag{A.1}$$

where n is the time step index. Now, the Hamiltonian can been broken up, $H =$

$T + V$, into a kinetic part, T, and a potential part, V, which includes the nonlinear self interaction term. The SSF method will solve the kinetic and potential parts separately. The benefit of the split-step method is that, since the potential energy operator is diagonal in position space and the kinetic energy operator is diagonal in momentum space, it is advantageous to solve the kinetic and potential problems separately. The basic algorithm of SSF is to propagate the wave function over a time step, Δt, first by propagating $\psi_n(x,t)$ using the potential operator over half a time step, then propagate using the kinetic operator over a full time step, and finally using the potential operator again over half a time step. In other words,

$$exp(-iH\Delta t) = exp(-iV\Delta t/2)exp(-iT\Delta t)exp(-iV\Delta t/2) + o(\Delta t^3). \tag{A.2}$$

Since the potential energy operator is merely a multiplicative operator in position space, it amounts to just a phase-shift of the wave function. Therefore, applying the first potential operator half-step yields an intermediary function,

$$g_n = exp(-i(V_{ext} + g|\psi_n|^2)\Delta t/2)\psi_n. \tag{A.3}$$

In order to apply the kinetic operator to this intermediary function, we first transform g_n into momentum space with a Fast Fourier Transform, yielding $\tilde{g}_n$. Then propagate $\tilde{g}_n$ using the free particle propagator, which amounts to another addition of a phase factor,

$$\tilde{g_{n+1}} = exp(-i\pi^2 k^2 \Delta t/2L^2)\tilde{g_n}, \tag{A.4}$$

where k is the momentum step, and $2L$ is the size of the spatial grid. Finally, $\tilde{g}_{n+1}$ is transformed back to position space and the second potential half-step is applied

to yield

$$\psi_{n+1} = exp(-i(V_{ext} + g|\psi_n|^2)\Delta t/2)g_{n+1}. \tag{A.5}$$

As seen in Eq. (A.2), this method is third order accurate in time. Note that there are other methods, such as the Crank-Nicholson method, which can be used to solve Eq. (2.9), both of which have their advantages. For instance, the SSF method treats derivatives exactly, it is convergent for large space steps, and can automatically include periodic boundary conditions. However, it can be slow, requiring two FFTs per time step, and it is sensitive to sharp changes in the potential. Crank-Nicholson, on the other hand, is stable and fast, but requires a larger spatial grid and periodic boundary conditions need to be enforced. The choice of one versus the other is clearly application dependent.

A.2 Shooting Method

The shooting method is used to compute the eigenvalues and eigenfunctions of Eq. (A.6),

$$\mu\psi = -\frac{\hbar^2}{2m}\nabla^2\psi + V\psi + g|\psi|^2\psi. \tag{A.6}$$

The basic idea is to solve Eq. (A.6) as a two-point boundary value problem (BVP) where the eigenvalue, μ, is also an unknown to be computed. First, Eq. (A.6) is written as a first order system by introducing the variables,

$$\begin{aligned} y_1 &= \psi, \\ y_2 &= \psi_x, \\ y_3 &= \mu, \end{aligned}$$

which yield,

$$\begin{aligned}
\frac{\partial}{\partial x} y_1 &= y_2, \\
\frac{\partial}{\partial x} y_2 &= 2y_1(-y_3 + V + N y_1^2), \\
\frac{\partial}{\partial x} y_3 &= 0.
\end{aligned}$$

The shooting method then solves the above system by starting from some initial guess for the solution, here we use the solution to the corresponding linear problem,

$$\mu_l \psi_l = -\frac{\hbar^2}{2m} \frac{\partial^2}{\partial x^2} \psi_l + V \psi_l, \tag{A.7}$$

as the initial guess. The shooting method then makes iterative guesses on one boundary condition until the second boundary condition is satisfied.

For example, to solve Eq. (A.6) for the first anti-symmetric eigenstate with a nonlinearity of 0.5, the BVP to be solved is,

$$\mu \psi = -\frac{\hbar^2}{2m} \frac{\partial^2}{\partial x^2} \psi + V \psi + 0.5|\psi|^2 \psi, \tag{A.8}$$

$$\psi(0) = 0, \tag{A.9}$$

$$\psi(\infty) = 0. \tag{A.10}$$

So, the function should be zero at $x = 0$ and decay to zero as $x \to \infty$. Finally, the shooting method would then vary the first derivative of the function, $\psi'(0)$, at 0, and integrate ("shoot") the solution to some value $x = x_0 \gg 0$ until the numerical solution approximately matches the second boundary condition, $|\psi(\infty) - \psi(x_0)| = \epsilon$ where ϵ is the error tolerance allowed. As an example of the method at work, Figure

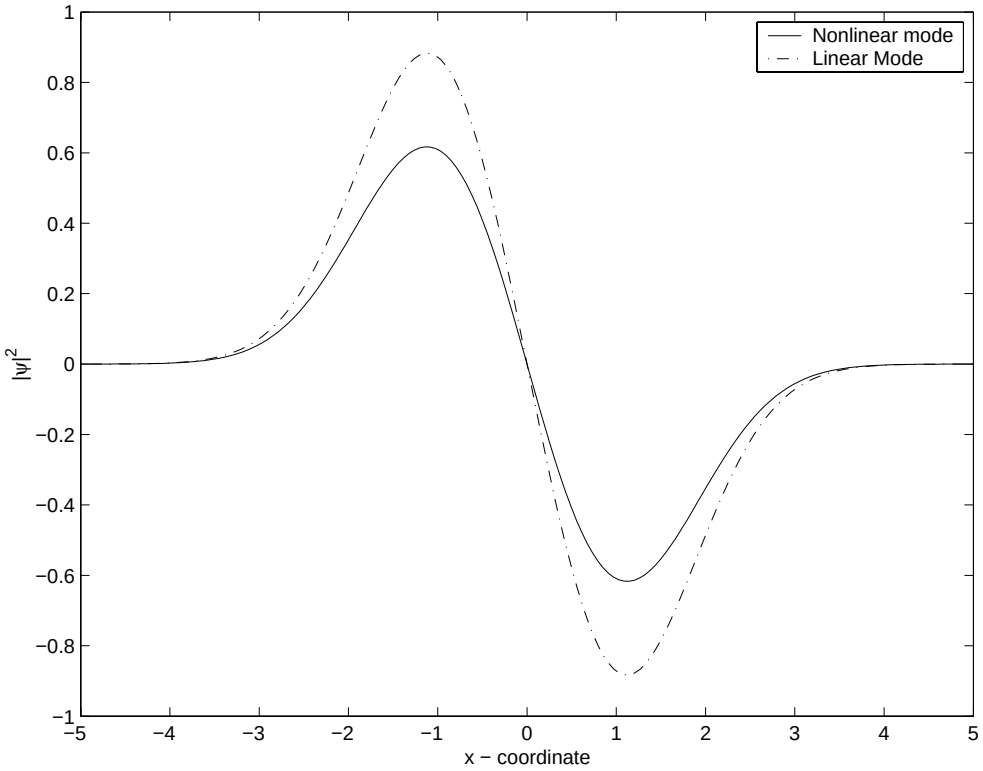

Figure A.1: The first anti-symmetric linear and nonlinear mode.

(A.1) shows the computation of the the first anti-symmetric mode. The computed linear and nonlinear eigenvalues are $\mu_l = 2.0532$ and $\mu = 2.1919$. Clearly, for weak nonlinearities the nonlinear mode does not differ greatly from the linear mode.

Bibliography

[1] S. Bose, Z. Phys. **26**, 178 (1924)

[2] A. Einstein, Sitzber. Kgl. Preuss. Akad. Wiss. 261 (1924)

[3] Y. Castin, e-print: cond-mat/0105058 v1 (2001)

[4] M. H. Anderson et al., Science **269**, 198 (1995)

[5] K.B.Davis et al., Phys. Rev. Lett. **75**, 3969 (1995)

[6] C. C. Bradley, C. A. Sackett, J. J. Tolett, and R. G. Hulet, Phys. Rev. Lett. **75**, 1687 (1995)

[7] H. London and F. London, Proc. Roy. Soc. (London) **A149**, 71 (1935)

[8] E. P. Gross, Nouvo Cimento **20**, 454 (1961).

[9] E. P. Gross, J. Math. Phys. **4**, 195 (1963).

[10] L. P. Pitaevskii, Sov. Phys. JETP **13**, 451 (1961).

[11] N. Bogoliubov, J. Phys. USSR **11**, 23 (1947).

[12] K. Huang, *Quantum Field Theory*, (John Wiley and Sons, 1998)

[13] C. Pethick and H. Smith, *Bose-Einstein Condensation in Dilute Gases*, (Cambridge University Press, 2002)

[14] L. I. Schiff, *Quantum Mechanics*, (Mcraw-Hill, 1955)

[15] B. Anderson and P. Meystre, Optics and Photonics News **20**, (June 2002).

[16] J. Stickney and A. Zozulya, Phys. Rev. A **66**, 053601 (2002)

[17] W. Hänsel, J. Reichel, P. Hommelhoff, and T.W. Hänsch, Phys. Rev. A **64**, 063607 (2001).

[18] J. Reichel, W. Hänsel, P. Hommelhoff, and T.W. Hänsch, Appl.Phys. B **72**, 81 (2001).

[19] J. Denschlag, D. Cassettari, and J. Schmiedmayer, Phys. Rev. Lett. **82**, 2014 (1999).

[20] D. Müller, D.Z. Anderson, R.J. Grow, P.D.D. Schwindt, and E.A. Cornell, Phys. Rev. Lett. **83**, 5194 (1999).

[21] N.H. Dekker, C.S. Lee, V. Lorent, J.H. Thywissen, S.P. Smith, M. Drndic, R.M. Westervelt, and M. Prentiss, Phys. Rev. Lett. **84**, 1124 (2000).

[22] M. Key, I.G. Hughes, W. Rooijakkers, B.E. Sauer, and E.A. Hinds, D.J. Richardson, and P.G. Kazansky. Phys. Rev. Lett. **84**, 1371 (2000).

[23] W. Hänsel, P. Hommelhoff, T.W. Hänsch, and J. Reichel, Nature **413**, 498 (2001).